Structures 61 (2024) 106003

Contents lists available at ScienceDirect

Structures

journal homepage: www.elsevier.com/locate/structures

Cyclic behaviour of an innovative cap beam to column pocketless connection in GFRP-RC precast structures

Mohamed H. El-Naqeeb [a,b,1], Tohid Ghanbari-Ghazijahani [c,2], Aliakbar Gholampour [d,3], Reza Hassanli [a,*,4], Yan Zhuge [a,5], Xing Ma [a,6], Allan Manalo [e,7]

[a] University of South Australia, UniSA STEM, Mawson Lakes, SA 5095, Australia
[b] Badr University in Cairo, School of Engineering and Technology, Cairo 11829, Egypt
[c] Macquarie University, Sydney, Australia,
[d] College of Science and Engineering, Flinders University, Tonsley, SA 5042, Australia
[e] Center for Future Materials, School of Engineering, University of Southern, Queensland, QLD 4350, Australia

ARTICLE INFO

Keywords:
Accelerated construction
Cap beam
Epoxy duct connection
GFRP
Prefabricated construction

ABSTRACT

This study examined the cyclic performance of innovative connection details for precast cap beam-to-column connections reinforced with glass fibre-reinforced polymer (GFRP). It aims to address the shortcomings identified in the performance of the previously examined pocket connections, where premature failure around the pocket was the governing failure mode, subsequently led to a reduced capacity. Three pocketless specimens were cast and assembled using epoxy resin and bolts/bars as connecting reinforcement in ducts (epoxy duct connection). Epoxy resin was used for its non-shrinkage properties and high early strength which can contribute to the acceleration of the construction process. A unique test setup that represents the cap beam-column connections in real-life scenarios where the beam at the joint end is free to rotate was used. The cyclic performance in terms of hysteresis behaviour, energy dissipation, stiffness, and residual drift was evaluated, and the results were compared to those of pocket connections. The test specimens exhibited a concrete failure at the column region away from the column end, indicating a strong connection with no sign of failure/slippage of the GFRP reinforcement. The proposed pocketless connection outperformed the pocket one, achieving a greater lateral capacity of 48%. It has the potential to prevent premature failures observed in pocket connections, relocating the failure from the connection region to the column. Additionally, the proposed epoxy duct connections dissipate more energy than the pocket connection and exhibit a low stiffness degradation rate with fewer residual deformations. This study concluded that the epoxy duct connection using epoxy resin and connecting reinforcement in ducts can be effectively utilized to assemble GFRP-RC precast structures with proper integrity of precast elements. The findings of this research can be used to accelerate the construction of GFRP-RC elements in aggressive environments, particularly in structures located in coastal regions, such as jetties.

1. Introduction

Fibre-reinforced polymers (FRPs) have gained increasing attention in the construction industry in recent years as a substitute for traditional steel reinforcement in concrete structures. The reinforcing steel can corrode especially in aggressive environments such as coastal regions, which adversely affects the structural performance [1] and imposes a significant amount of cost due to inspection, maintenance and

* Corresponding author.
E-mail address: reza.hassanli@unisa.edu.au (R. Hassanli).
[1] ORCID: https://orcid.org/0000-0002-0573–2978
[2] ORCID: https://orcid.org/0000-0002-8743–739X
[3] ORCID: http://orcid.org/0000-0001-5069-2963
[4] ORCID: https://orcid.org/0000-0001-5855-6405
[5] ORCID: http://orcid.org/0000-0003-1620-6743
[6] ORCID: http://orcid.org/ 0000-0001-5488–5252
[7] ORCID: https://orcid.org/0000-0003-0493-433X

https://doi.org/10.1016/j.istruc.2024.106003
Received 3 December 2023; Received in revised form 17 January 2024; Accepted 30 January 2024
Available online 7 February 2024

rehabilitation [2]. The noncorrodible nature of FRP is one of their key advantages over steel reinforcement, as it eliminates the costly damages caused by steel corrosion in concrete structures [3] and ensures a sustainable structure with a less negative impact on the environment [4]. In addition, FRP has a higher strength-to-weight ratio than steel that can provide ease of installation [5]. In contrast, FRP has a lower modulus of elasticity compared to steel and behaves in an elastic manner which results in relatively larger deformation and lower energy dissipation in the FRP- FRP-reinforced concrete (RC) compared to the steel-RC counterparts [6]. Although the viability of utilizing FRP in RC elements was demonstrated in previous studies [7–10], the studies on the connections of these elements are limited.

Beam-column connections are critical regions that govern the overall performance and stability of cast-in-place [11] and precast RC structures [12] because they are often the weakest point in the frame and suffer a strong discontinuity in the strain field as well as concentrated stresses compared to the connected beams and columns [13]. Several studies investigated the behaviour of cast-in-place FRP-RC connections, according to which the glass FRP (GFRP)-RC beam-column connection exhibited mainly elastic behaviour until failure and showed an acceptable drift response [14,15]. However, the GFRP-RC connection demonstrated lower energy dissipation capability compared to the conventional steel reinforcement due to its linear elastic behaviour in comparison to the elastic-plastic behaviour of steel [14]. The contribution of the transverse beam and slab floor to the cyclic behaviour of the GFRP-RC beam-column connection has been also assessed in previous studies [16,17]. It has been found that the contribution of the slab floor is more pronounced with increasing the size of the transverse beams due to improving the contribution of slab bars [16,17]. Moreover, confining the joint region by an internal FRP tube [18] or inclined bars at the connection corners [19] proved its efficiency in improving the energy dissipation of GFRP-RC beam-column connections.

Precast concrete structures are becoming increasingly popular due to their many advantages, such as speed of construction, improved quality control, and reduced environmental impact [20]. Additionally, precast construction reduces on-site labour and lowers health and safety risks [21]. In precast concrete construction, beam-column connections are critical components that play a vital role in the overall behaviour and integrity of the structure [12]. Based on the load transfer mechanism, precast connections can be classified into different types. Pocket and socket connections involve embedding precast columns into beams for efficient construction and enhanced structural performance, with the former utilizing a partially precast column and the latter using a fully precast column [22]. Mechanical bar splices are utilized to minimize reinforcement's development length and to lower construction costs [23]. On the other hand, bolts and prestressed tendons offer the advantage of repairability after earthquakes. Bolts are key for energy dissipation but require replacement [24]. Grouted duct connections are gaining importance in earthquake-resistant precast concrete structures. This method involves inserting reinforcement bars from one element into ducts in the other element, offering comparable strength and ductility to cast-in-place connections with faster assembly [25]. Understanding the performance of the structural connections is important in their effective and safe design.

Numerous studies have been conducted to propose and examine innovative and efficient connections for precast steel-RC connections. Ghayeb et al. [26] evaluated the cyclic performance of a new hybrid connection using steel tubes, plates, and couplers to join beams and columns. The results demonstrated that the proposed connections meet seismic requirements, allowing their use in high seismic zones. Additionally, Zhang et al. [27] proposed a dry precast beam-column connection that is easy to assemble and disassemble and facilitates component upgrading and replacement. The results revealed that the precast connection has a capacity like the cast-in-place one. Moreover, the pocket connection utilized a noncontact lap splice, and ultra-high performance concrete (UHPC) proved its proper performance in terms of capacity, energy dissipation, and damping ratio [28]. Tazarv and Saiidi [29] found that the duct diameter has a significant impact on the development length of bars in UHPC-filled duct connections. Also, both the duct/bar diameter ratios and embedment length affect the maximum nominal bar stress in monotonic pull-out tests, while embedment length influences the specimen failure mode [30]. Furthermore, the capacity of grouted duct connections with a large reinforcement diameter was found similar to the corresponding connection using grouted sleeve [31]. However, the pinching behaviour of the connection was more pronounced after a drift ratio of 2% due to the bar slippage. An improved grouted duct connection was proposed by Wang et al. [32]. It has been found that the proposed grout duct connection behaves similarly to the corresponding cast-in-place connection.

While several studies have been conducted on the behaviour of connections in precast steel-RC, studies on the precast FRP-RC are limited. Design standards for precast GFRP-RC connections are still out of the scope of international design codes due to the lack of enough knowledge in the area [33]. Due to the inherent differences between FRP and steel which were discussed earlier, the findings of the previous studies on precast steel-RC cannot be adopted for FRP-RC members. Therefore, there is an urgent need for further investigation in this area to bridge the knowledge gap and ensure the reliable and effective use of FRP reinforcement in precast concrete structures. Recently, the cyclic behaviour of dry precast GFRP-RC connections with GFRP bolts was evaluated [34]. The results revealed that the precast connections with GFRP reinforcement and using GFRP bolts performed satisfactorily by preventing brittle failure [34]. Additionally, a new connection for precast GFRP-RC pocket connections was developed, where the column was connected to the beam elements through beam pockets which were filled with epoxy resin [35]. Although epoxy used in the pocket had advantages including high strength, non-shrinkage properties, high workability, and faster assembly of the structure, its relatively low modulus of elasticity negatively affected the connection performance. This resulted in larger stress concentrations, leading to the localization of stresses in the column at the pocket location and consequently immature failure of the column [35]. To overcome the premature failure in the pocket region, it was recommended to provide a minimum column embedded depth of 1.4 times the column cross-section thickness. Additionally, proper confinement of the pocket by concrete is essential, with a minimum thickness equal to 0.5 times the column cross-section thickness from the bottom and sides [36]. The behaviour of large-scale GFRP-RC frames with different connection detailing have also been examined in previous studies [37,38]. The improved performance of pocketless connections compared to pocket ones in terms of capacity, damping ratio, and energy dissipation was reported in the literature [38].

This study is part of a large project that aims at developing effective and efficient precast construction connections that can meet a range of performance requirements. Its major aim is to address several key issues related to precast construction, including corrosion, construction cost, structural resilience, and sustainability. While previous studies have examined the behaviour of dry and pocket connections in GFRP-RC precast connections, there has been no investigation of the behaviour of pocketless connections. Although previous studies reported that the failure mode of pocket connections was localized at the pocket due to the stress concentration [35], pocketless connections can potentially overcome the problem of stress concentration in the beam. Pocketless connections allow for a more uniform stress distribution along the length of the bars, as well as providing structural integrity with minimum bonding material and minimum on-site waste. The manufacturing of formworks is also less complicated due to the lack of pockets in the beams. In the current study, pocketless connections in the form of epoxy duct connections are used to connect the beam and column using epoxy resin. This connection is from the category of grout duct connection while replacing the conventional grout with epoxy resin. Epoxy resin was employed to overcome the existing challenge in the construction industry of accelerating the building process. This allowed for the

achievement of high initial strength, along with non-shrinkage properties and sufficient workability. Various GFRP connectors were employed in this study, including sand-coated bars, bolts, and prestressed bolts. The detailing of these types of connections is simpler than the traditional pocket connections, which makes the manufacturing process easier. The evaluation of the cyclic performance of the tested specimens in terms of hysteresis curves, stiffness, damping ratio, energy dissipation, and residual drift is evaluated. Additionally, the performance of the proposed connection is compared to typical pocket connections reported previously. The findings of this research can be used to accelerate the construction of GFRP-RC elements in coastal region structures and jetties.

2. Experimental program

2.1. Specimens' details

This experimental test is part of an ongoing research project that examines the behaviour of different types of precast GFRP-RC connections. The project primarily focuses on the behaviour of cap beam-to-column connections in precast concrete jetty structures, where the use of GFRP reinforcement is considered as effective and durable. A total of six pocket connections with different detailing were tested previously [35]; however, all were reported to experience some levels of premature failure in the beam due to stress concentration around the pocket region. To enhance the connection performance and prevent stress localization in the beam, pocketless connections with epoxy duct connections were introduced and examined in this study. The specimens were designed and fabricated using precast concrete beams and columns in the form of connecting reinforcement through ducts, which is called epoxy duct (ED) connection. In the ED connection reported here, ducts were prefabricated in both the precast column and beam element during the manufacturing stage. GFRP connecting reinforcements were inserted into the duct during the structure assembly. Due to the brittle nature of GFRP bars, if the bars protrude from the precast column, they pose risks during transportation and construction stages, as the bars can fail. Hence, the connections were designed in a way that no GFRP bars stick out of the precast concrete, and the segments are connected through connection bars on-site. The epoxy adhesive was then injected into the duct, filling any gap and providing a bond for the connecting GFRP reinforcement inside the column and beam. Epoxy was used instead of cement-based grout due to its high early strength and non-shrinkage properties. Also, it has significantly higher strength than traditional grouting materials and can develop strength faster, allowing for quicker curing times, easier construction, and earlier use of the structure. The reinforcement details of the tested specimens are shown in Fig. 1. The dimensions and reinforcement of both column and beam were kept constant in the three specimens. Except for the connection region, the general dimensions and reinforcement detailing were kept similar to the pocket connections tested previously.

The test specimens were designed according to the design guidelines (ACI 440.1R-15) [39] for both shear and bending. Column and beam cross-sections were designed to fail due to concrete failure. Sufficient margins were ensured between the calculated bar strains and the rupture strains of the GFRP reinforcement to mitigate the possibility of brittle failure due to bar rupture. The columns had a cross-section of 200 mm by 200 mm and a length of 1500 mm. The columns were longitudinally reinforced by four GFRP bars with a diameter of 16 mm, as well as transverse reinforcement in the form of closed GFRP ligatures with a diameter of 10 mm spaced 70 mm apart. The beam and column cross-sections were maintained identical to those in the first part of this project [35] to allow for a direct comparison between the pocket and pocketless connections. The beam had a cross-section of 400 mm by 320 mm and a length of 1500 mm. It was reinforced with three GFRP bars with a diameter of 13 mm as bottom and top reinforcement and closed GFRP ligatures with a diameter of 10 mm spaced 100 mm apart as transverse reinforcement. It should be noted that the cap beam size

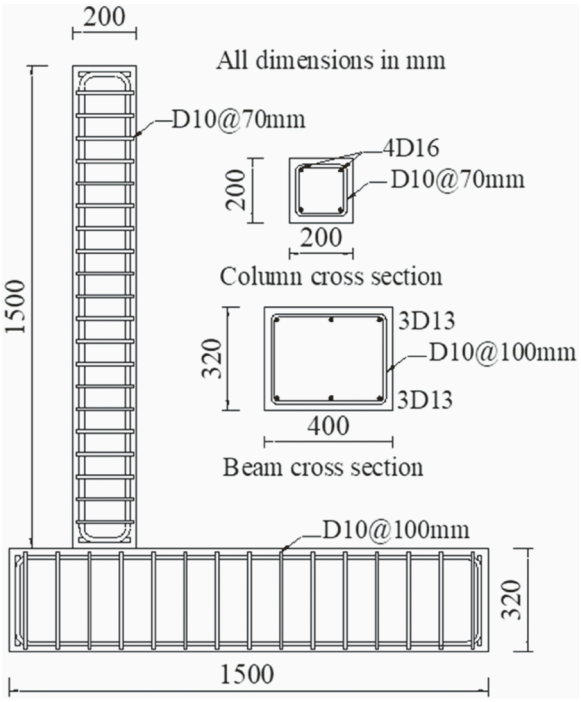

Fig. 1. Dimension and reinforcement of the tested specimens (dimensions in mm).

was intentionally set larger than the column, with greater breadth, to simulate jetty structures and also accommodate and provide the necessary confinement to the embedded depth of the column through the pocket in the first part of this project [35].

The specimens were designed to investigate the effect of the type of connectors (GFRP bars and GFRP bolts) as well as the pre-stressing. The connection's detailing is presented in Fig. 2. The connections were made using connection bars/bolts placed in the ducts of beams and columns which were filled with epoxy resin to provide a rigid beam-column connection to enable transferring moment. The specimens in this study include ED1, which utilizes four GFRP sand-coated bars of diameter 19 mm as connectors; ED2, which uses a GFRP bolt of diameter 22 mm as connectors; and ED3, which is identical to ED2 but with a nut at the end of the bolt to apply and hold pre-stressing force of 30 kN, which is around 5% of the ultimate tensile strength of the bolts. By analysing the performance of these different connections, this study can provide insights into the optimal design of precast beam-column connections using connecting GFRP reinforcement; bars/bolts.

2.2. Manufacturing of precast concrete elements

Fig. 3 illustrates the various stages of specimen manufacturing, including Fig. 3-a which depicts the construction stage and Fig. 3-b which shows the specimens during the curing process prior to beam-column assembly. Proper positioning and fixation of the reinforcement cages were crucial to maintain their correct location during concrete vibration because of the buoyancy effect of the GFRP reinforcement. This was achieved using ties and small GFRP seats to secure the cages to the formwork. Steel shafts with a diameter of 32 mm were inserted in the formwork to create empty ducts for the placement of the connection reinforcement. The steel shafts were greased to prevent bonding with the concrete and avoid damage to the surrounding concrete during removal. The concrete for the beam and column elements was cast at the same time, and after approximately 12 h, the shafts were removed. After 48 h, the formworks were de-moulded. The specimens were then wrapped in plastic covers and cured in an ambient environment to ensure proper curing of the beam and column elements before assembly.

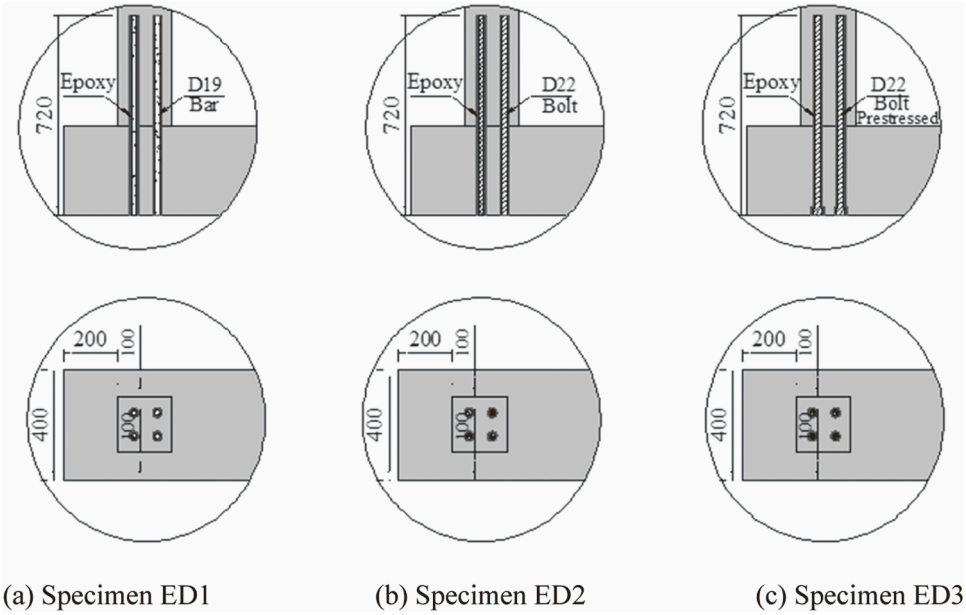

Fig. 2. Details of the proposed connections (dimensions in mm).

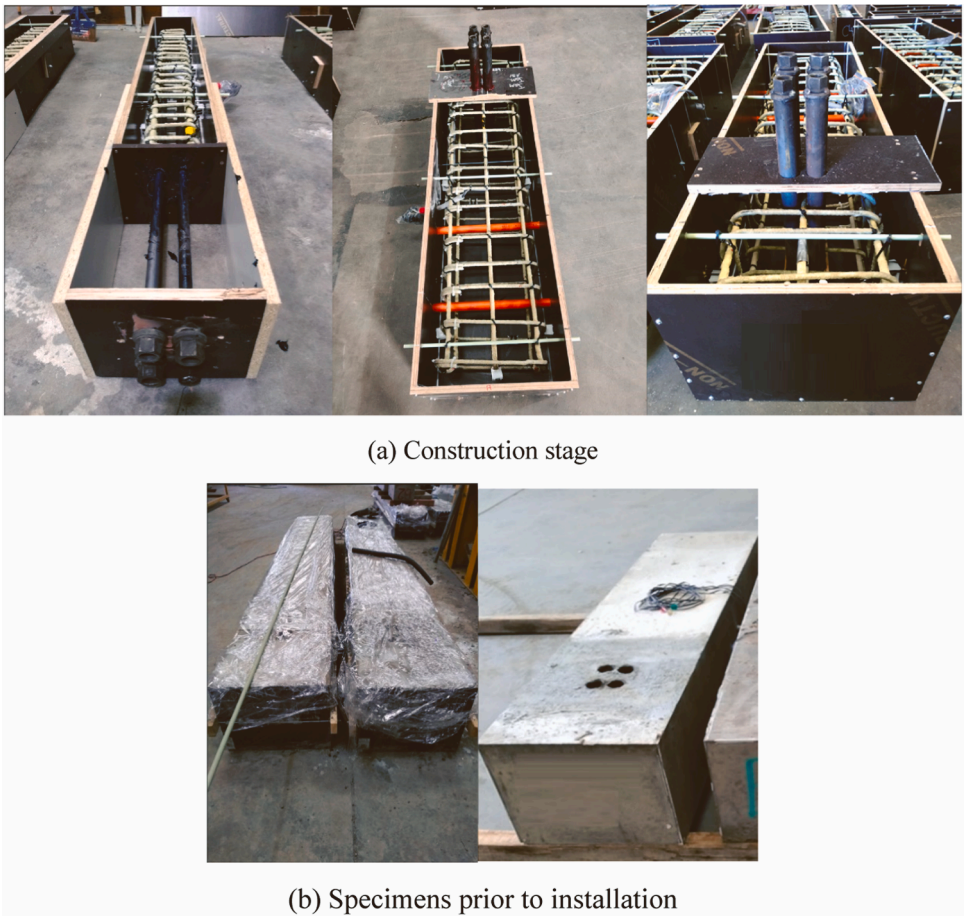

Fig. 3. Construction stages for precast elements.

2.3. Specimens assembly

The assembly process of the test specimen involved several steps, as shown in Fig. 4. First, the columns were placed upside down and the epoxy was used to fill the designated holes in the columns for the connection reinforcement. The connection reinforcement was then inserted into the ducts. The beams were placed at an elevated height to facilitate access to the holes from the beam soffit. After 24 h, the beam

Fig. 4. Assembly of tested specimens.

ducts were filled with epoxy, the columns were lifted using a forklift and positioned through a set of pre-designed holes on top of the column. Great care was taken to ensure that the columns were safely and accurately placed on the beams. For the pre-stressed connection, the stress was applied by tightening a nut from the bottom of the beam resulting in a pre-tensioning of 30 kN in the bolt. After applying the stress, the beam ducts were filled with epoxy.

The use of two wood braces to diagonally link beams to columns (see Fig. 4) during curing helped to hold the column in the intended position and orientation, ensuring that it was perpendicular to the beam. To join the bracing to the specimens, several threaded rods were used through holes that were pre-designed in the columns and beams.

2.4. Test setup

Fig. 5 shows the unique test setup that represents the cap beam-column connections in real-life scenarios, where the beam at the joint end is free to rotate. To achieve this, a steel framework was created to elevate the specimens from the strong floor, which allowed for a suitable overhang for the beam-column connection to allow for rotation. To secure the beam at the fixed end, the set-up included four triangular plates (PL400 ×290 ×20) and two universal beam sections (310UB46), as well as a variety of minor connecting components as shown in Fig. 5. The beams were secured in their position on the steelwork using toe clamps and high-strength bolts. Soft rubber was used as a filler beneath the clamps to provide a uniform distribution of the clamping force and prevent early failure owing to stress localization. The loading ram was attached to the upper end of the column using two plates of dimensions 400 × 300 mm and 20 mm thickness along with four high-strength bolts.

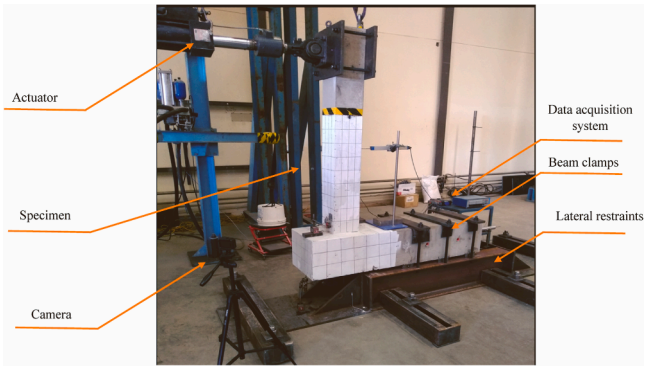

Fig. 5. Test setup details.

2.5. Instrumentation and applied load

The data was loaded, acquired, and processed using a computerized system. The displacements of the specimens at several locations were measured using displacement transducers (LVDTs) with various strokes as presented in Fig. 6. Two LVDTs were utilized to record the displacement at the mid-height and the top of the column, one was attached to the beam's fixed end to capture the lateral displacements in the direction of loading. Another LVDT was positioned on the beam's bottom surface and below the joint area, to record the downward and upward displacement of the beam's end relative to the strong floor.

The test connections represent a cap beam-to-column connection in jetties. These structures are primarily designed for lateral loads, with axial loads being of minor consideration. To consider the most critical loading scenario, the specimens were tested under lateral cyclic loads without the application of axial loads. It is worth noting that the presence of axial load can have a beneficial effect on enhancing connection confinement and, consequently, improving connection capacity. The lateral cyclic loading was applied in a displacement-control regime using a 100-kN MTS actuator with a maximum stroke of ± 150 mm. The ASTM-E2126 Method B standard test procedure was followed [40] for the loading as shown in Fig. 7. The loading system was designed to receive input from a total of 44 cycles, all of which had a constant displacement rate. The initial five cycles had an incrementally increasing displacement. Subsequently, three fully reversed and repeated cycles at increasingly larger displacements were applied. Unless a significant failure occurred or the machine reached its max stroke, the loading was continued. Furthermore, to make sure that the tests were carried out in a quasi-static state, the loading speed was restricted to 0.6 mm/s. This indicates that the loading was slow enough to allow the specimen to deform and respond to the load in a controlled manner.

3. Properties of materials

Concrete cylinders were cast using the same batch of concrete that was used to construct the test specimens. The standard concrete cylindrical samples (height × diameter: 200 ×100 mm). The compression tests were conducted at the same time as the specimen testing. The average compressive strength of the concrete from these tests was 82.4 MPa, with a standard deviation of 0.8 MPa. High-strength concrete was chosen to maximize the advantages of the increased strength of GFRP reinforcement, as compression failure of concrete typically governs the failure of GFRP-RC sections. In addition, high-strength concrete is usually used in the construction of offshore structures [41]. The properties of the used GFRP reinforcement and bolts, as provided by the supplier, are listed in Table 1. Moreover, according to the manufacturer, the epoxy used to anchor the GFRP bolts inside the holes had

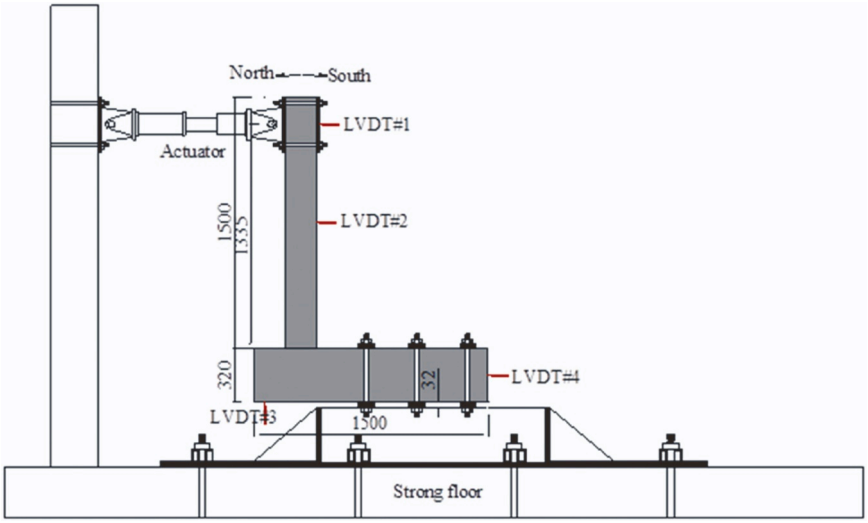

Fig. 6. LVDT locations and test setup (All dimensions in mm).

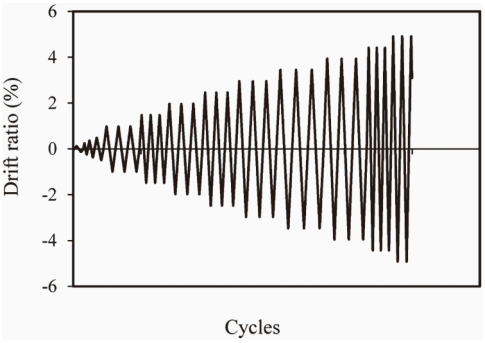

Fig. 7. Loading protocol.

compressive and tensile values of 93.5 and 12.1 MPa, respectively.

4. Test results and discussion

4.1. Cracking propagation and failure of specimens

Fig. 8 shows the cracking progression and failure of the test specimens. The general behaviour of all specimens was more or less the same. At the early stage of loading, all three specimens exhibited horizontal hairline cracks at the base of the column. At a drift of about 3%, a hairline crack was detected in the beams of specimens ED1 and ED2 while it was noticed at an earlier drift of about 2.2% for specimen ED3, which was propagated from the top surface of the beam at the south side of the column, as shown in Fig. 8. After a few cycles of reversed loading, these beam cracks extended to the bottom of the beam at a drift ratio of about 5.5% in specimens ED1 and ED2 while this happened at a drift ratio of about 3.5% in specimen ED3. The width of this crack remained relatively small until the end of the test. In addition, the column cracks started to initiate at a drift ratio of about 4.5% in specimens ED1 and ED2 while it happened at a drift ratio of 3.5% in specimen ED3. These cracks were formed at 50–200 mm above the column base and were followed by the formation of severe longitudinal (vertical) cracks parallel and along the length of the connection reinforcement. The final failure mode in all the specimens was column failure characterized by concrete crushing along the length of connection reinforcement and above the column base by 100 mm in specimens ED1 and ED2 and 50 mm in specimen ED3 (see Fig. 9). After the test, the specimens showed no signs of failure in GFRP bars, neither longitudinal nor stirrups. No failure of the reinforcement was observed in the beams, columns and connection regions. It is worth mentioning that the obtained failure mode differs from the failure model of similar-sized specimens with pocket connections in which the failure was observed at the pocket connection in a previous study [35]. This will be discussed in detail in the next section.

The cracks developed on one side of the beam are due to the boundary conditions of the test setup. The test setup was mainly designed to simulate the real-life scenarios of the cap beam-to-column connection of jetty frames, the connection represented one corner, allowing the beam to be free to rotate as in the real-life situation. This test setup led to beam cracks at the side of the beam where the beam was clamped. With updates to the test setup, i.e., considering interior connections similar to those in building structures, the boundary conditions should be modified, subsequently, resulting in more restriction on the beam rotation and hence a different performance crack behaviour.

4.2. Load–drift hysteresis behaviour

The hysteresis behaviour of the specimens is shown in Fig. 10. The drift ratio is calculated as the ratio between the column displacement at the top divided by the distance between the load application point to the

Table 1
Properties of GFRP reinforcement.

Bar No.	Nominal bar diameter (mm)	Nominal cross-section Area (mm^2)	Tensile Modulus of Elasticity (GPa)	Ultimate Tensile Strength (f_{fu}) (MPa)	Ultimate strain in tension (ε_{fu})
D 10	9.5	71	62.50	1315	0.023
D 13	12.7	129	61.30	1282	0.021
D 16	15.9	199	60.00	1237	0.021
D 19	19.1	284	60.50	1270	0.021
Bolt #22	22.2	387	46.20	625	0.015

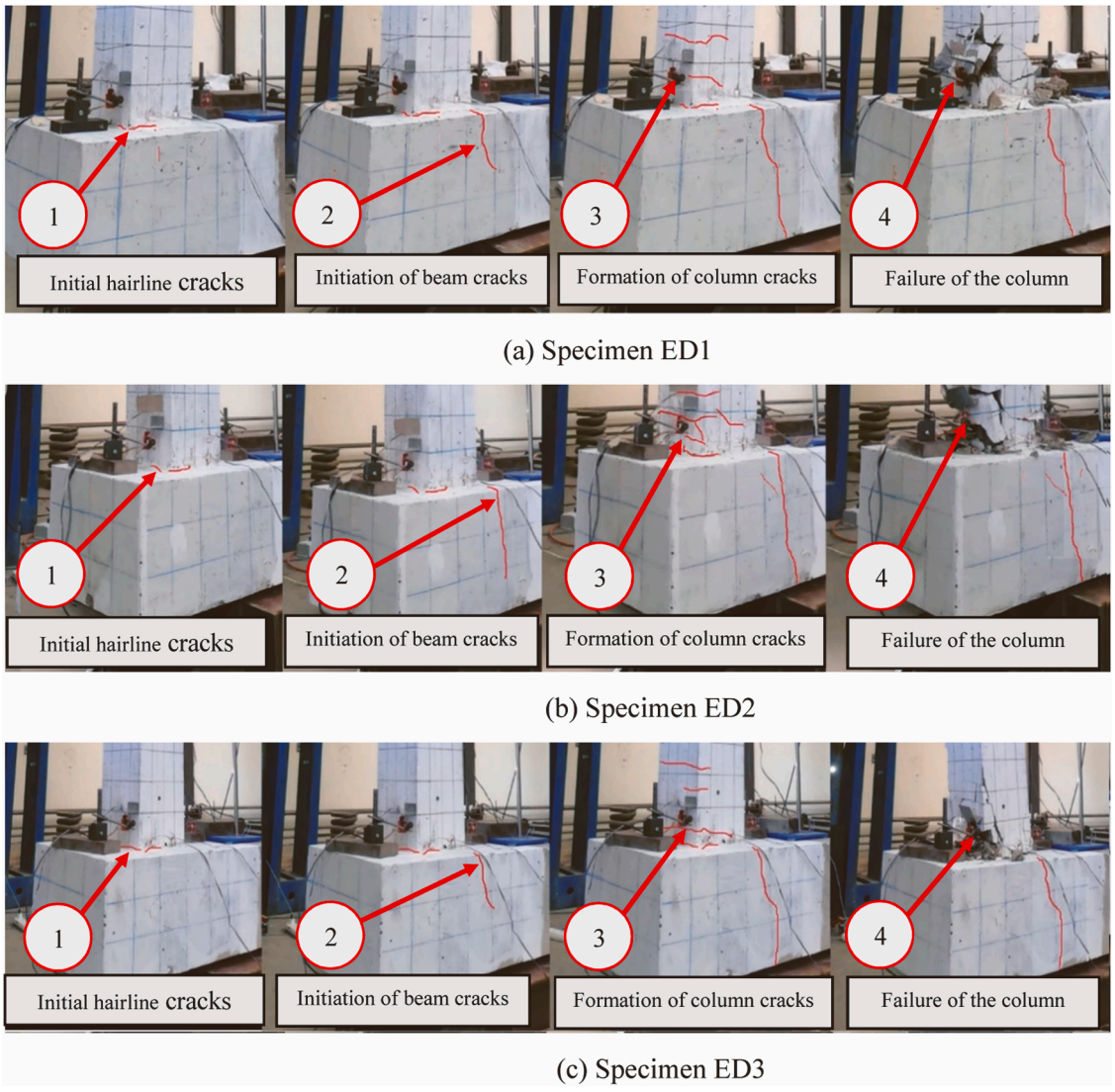

Fig. 8. Cracks propagation in specimens ED1, ED2 and ED3.

column base as shown in Fig. 6 (= 1.335 m). Based on Fig. 10, the specimens exhibited unsymmetrical responses in both the push (away from the actuator) and pull (towards the actuator) directions due to the unsymmetrical geometry of the specimens. The envelope curves are shown in Fig. 11 and the peak capacities in push and pull directions as well as the average capacities are presented in Table 2.

For specimen ED1, the maximum load capacity in the push direction was 19.6 kN which was slightly higher than that in the pull direction (19.2 kN). This can be due to two reasons. The first reason is that the damage caused in the push direction resulted in a reduced load in the pull direction. The second reason is due to the unsymmetrical geometry of the specimen in the north and south directions of the column and the formation of beam cracks at the south side of the column. In both pull and push directions, the load peaked at a drift ratio of about 4.9%. Up until the peak points, the hysteresis loops were very narrow owing to the linear elastic behaviour of GFRP reinforcement. However, beyond the peak points, the hysteresis loops became wider, due to the formation of cracks as well as spalling and crushing of concrete.

The general behaviour of specimen ED2 was similar to that of specimen ED1. However, the difference of the behaviour in push and pull direction became more significant in specimen ED2 compared to the other two specimens where a maximum load of 21.4 kN in the push direction was obtained at a drift ratio of 5.7% while the peak load in the pull direction was 19.2 kN which was 10% lower and occurred at a drift of 4.9%. Although the amount of connection reinforcement in specimen ED2 was 35% greater than that of specimen ED1, the improvement in the connection capacity was observed in the push direction only and was limited to 9% compared to that of specimen ED1. Meanwhile, the capacity in the pull direction was almost the same for both specimens.

The maximum load capacity of specimen ED3 in the push direction was 17.7 kN and was obtained at an earlier drift ratio of about 4.0% while the maximum load capacity in the pull direction was 17.4 kN corresponding to a drift ratio of about 4.4%. Even though both specimens ED2 and ED3 were identical, except that the connection reinforcement was prestressed in specimen ED3. This reduction in the capacity is controlled by the connection flexibility caused by the reduced beam rotation. The effect of beam rotation on the connection capacity will be discussed in the following sections. While the inclusion of a nut was intended to ensure effective anchorage for the reinforcement, it appears to have impacted the load transfer through the connection reinforcement by reducing the effective length participating in transferring the load through the surface area of the bolt, thus adversely affecting the connection performance. This observation is also believed to have occurred due to the induced internal movement and potential micro-cracking/debonding of epoxy due to the prestressing force in the bolts. The same observation was also reported in pocket connections,

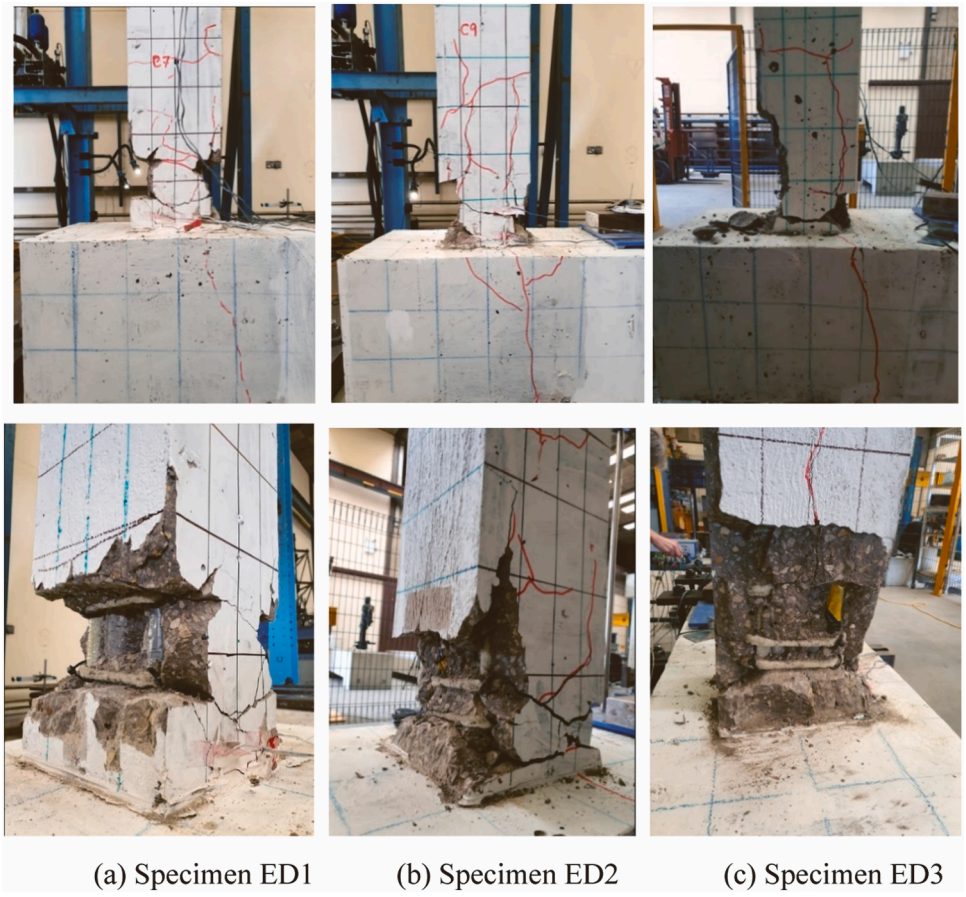

Fig. 9. Final failure of specimens ED1, ED2 and ED3.

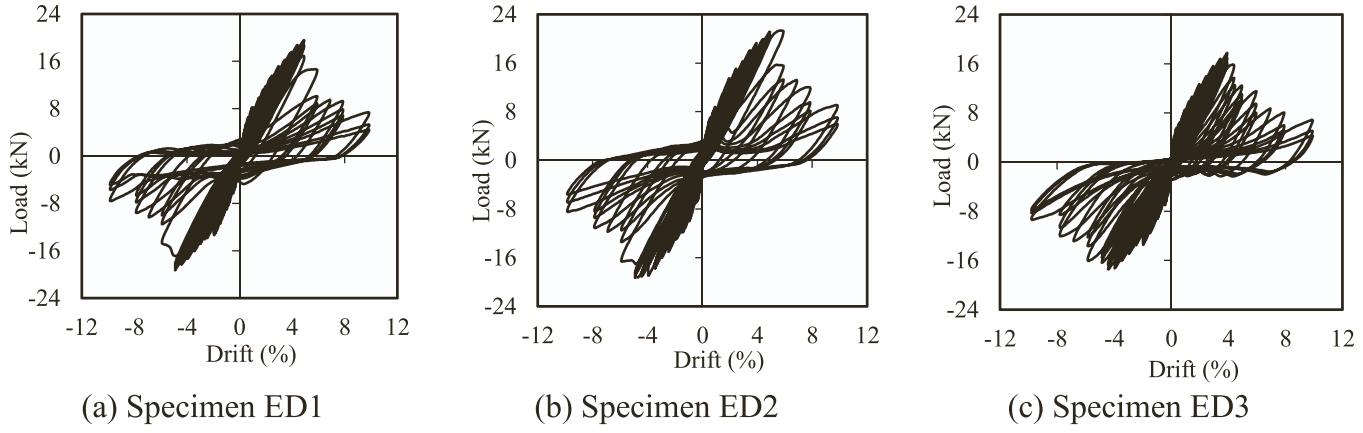

Fig. 10. Load-drift hysteresis.

where a connection with a prestressed central bolt, including a nut, exhibited reduced capacity compared to an identical non-prestressed one without a nut. [35].

The results confirmed that the test specimens were able to achieve a drift of 4%. While GFRP is a brittle material, its characteristics in terms of high tensile strength along with low modulus of elasticity enable the structures to undergo large deformations and concrete tensile cracking, followed by progressive crushing of the concrete in compression. Such pseudo-ductile behaviour provides warnings of impending failure. While seismic provisions in design standards are very limited, the Canadian standards for FRP-RC structures (CSA/S806–12) [42] require that deformable moment-resisting frames reinforced with GFRP should be capable of resisting a 4% drift without a reduction in strength. Therefore, the performance of the connections satisfied the design criteria.

The envelope curves shown in Fig. 11 indicate that at early loading stages, the three specimens followed a typical response with similar initial stiffness followed by nonlinear behaviour up to the maximum lateral capacity caused by damage initiation due to the formation of tensile cracks as well as the concrete undergo nonlinear behaviour with increasing the concrete strain. Specimen ED2 had the largest lateral capacity due to the provision of connection reinforcement with a greater cross-sectional area. The significant variation in the maximum lateral capacity, corresponding drift ratio, and the point at load drop in the

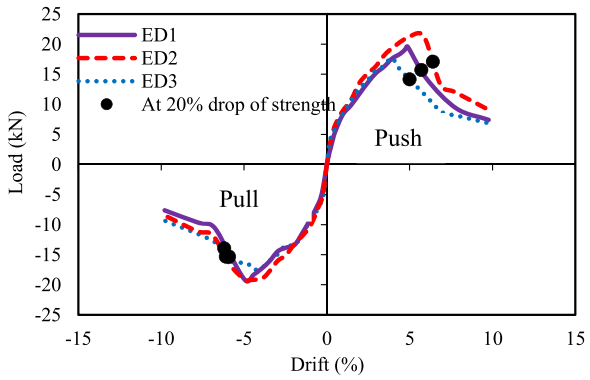

Fig. 11. Envelope curves of specimens ED1, ED2 and ED3.

Table 2
Capacity of specimens.

Specimen	Push capacity (kN)	Pull capacity (kN)	Average capacity (kN)
ED1	19.6	19.2	19.4
ED2	21.4	19.2	20.3
ED3	17.7	17.4	17.6

strength by 20% is more noticed in the push direction for the three specimens. On the other hand, the maximum lateral capacity of the three specimens in the pull direction was almost the same and occurred at the same drift ratio. Although the capacity of specimen ED3 is the lowest among the three specimens and occurred at an earlier drift ratio, the drift at a 20% drop in the pull direction was approximately the same in all specimens. In general, all specimens could withstand large drift ratios of up to 4.0% without experiencing a drop in strength. However, the specimens showed a greater lateral load capacity in the push direction than in the pull direction which can be explained by the location of the column with respect to the beam as well as the formation of beam crack at the south side of the column.

4.3. Energy dissipation and damping ratio

The accurate evaluation of the energy dissipation of GFRP-reinforced concrete is very important when it comes to seismic performance, especially considering the linear elastic behaviour of GFRP bars. The cumulative energy dissipation can be estimated by summing up the energy dissipated in successive load-displacement cycles. The energy dissipated during each cycle can be expressed as the area enclosed by the hysteretic loop under consideration. Fig. 12-a presents the cumulative energy dissipation in the first cycle of each loading step. The results indicated that the cumulative energy dissipated by all the specimens followed a similar trend because the three specimens exhibited a similar failure mechanism. It is evident from the results that the three specimens underwent comparable levels of energy dissipation up to a 4.0% drift ratio. However, the dissipated energy at the end of the loading differed among the specimens where both specimens ED1 and ED2 showed greater energy dissipation capacity compared to specimen ED3. Furthermore, the results show a significant correlation between the amount of energy dissipated through the hysteretic action and the degree of damage observed during the test. The slope of the relationship between the cumulated energy dissipation and the drift ratio for each specimen consistently rises towards the point of failure which indicates a higher rate of damage to the concrete due to concrete spalling and crushing.

The equivalent viscous damping ratio is another critical index for assessing the amount of hysteretic energy dissipation in reinforced concrete structures. Viscous damping provides a more complete picture of how the system behaves under cyclic loading conditions compared to energy dissipation alone because viscous damping is a dimensionless size-independent parameter. By providing information about energy dissipation, stability, and ability to resist further loading, damping can help to address some of the shortcomings of energy dissipation in characterizing the behaviour of a system. Fig. 12-b shows the equivalent viscous damping ratios, denoted as ζ_{eq}, for the first cycle of the loading step corresponding to the drift ratio.

The viscous damping values were determined for the specimens using the method described by [43] according to Eq. (1),

$$\xi_{eq} = \frac{E_d}{4\pi . E_e} \tag{1}$$

where E_d is the energy dissipation per cycle and E_e is the elastic energy in the system.

As shown in Fig. 12(b) at early loading stages up to 1% drift, as the drift ratio increased, the viscous damping, ξ_{eq}, also increased, primarily due to the initiation of tensile cracks in the column. However, at around 1% drift, ξ_{eq} decreased to approximately 3% and remained relatively unchanged until a drift ratio of 4–5%. The already-developed cracks did not contribute much to energy dissipation and hence it remained relatively unchanged at this level of drifts. Once the specimen ED3 reached a 4% drift ratio and the other two specimens reached 5% (which

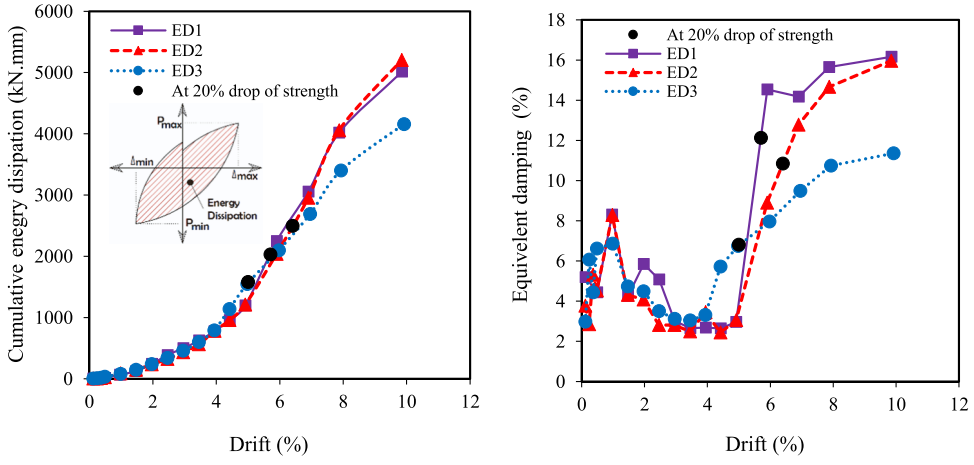

(a) Energy dissipation (b) Equivalent damping

Fig. 12. Energy dissipation and equivalent damping ratio.

corresponds to the point of maximum capacity), the viscous damping increased rapidly indicating increases in dissipated energy as a result of concrete spalling and crushing.

At the failure point where the strength drops by 20%, specimen ED2 exhibited the highest cumulative energy dissipation and damping ratio, followed by ED1. While specimen ED3 displayed the lowest cumulative energy dissipation and damping ratio. These results reveal that the specimen ED2 with greater joint reinforcement gives a better capacity to dissipate energy and resist damage under repeated loading compared to the other two specimens. This is attributed to the higher lateral capacity of this specimen at the same drift compared to the other specimens. Moreover, compared to ED2, the cumulative energy dissipation of ED1 was approximately 81.24% and the damping ratio was approximately 88.81%. This indicates that ED1 dissipated less energy and had a lower damping ratio compared to ED2. Similarly, compared to ED2, the cumulative energy dissipation of ED3 was approximately 63.15% and the damping ratio was approximately 62.8%. However, both specimens ED2 and ED3 were identical except for the prestressing force. The results confirm that the provision of prestressed bolts in ED3 led to the least dissipated energy and the lowest damping ratio compared to both ED1 and ED2.

4.4. Stiffness deterioration

The reduction in stiffness of specimens when subjected to quasi-static loading is commonly determined by examining the changes in the secant stiffness of load-displacement curves. However, in cyclic loading tests where the push and pull peaks of each cycle are connected, the resulting line does not intersect the origin. In this study, effective stiffness was employed to assess stiffness degradation in the specimens during cyclic tests. The effective stiffness was determined by calculating the slope of the line connecting the push and pull peak loads at each drift ratio. Fig. 13 shows the stiffness degradation of the three specimens at different drift ratios. The decrease in lateral stiffness followed a typical trend under different drift ratios due to the cracking of concrete. As the lateral load increased, the damage to the columns became increasingly severe, resulting in concrete spalling and crushing, which further contributed to the degradation of stiffness at larger displacement levels. Among the specimens, specimen ED3 had higher initial stiffness by 28% and 66% compared to specimens ED2 and ED1, respectively. However, the rate of stiffness deterioration for specimen ED3 at early drift ratios up to 1% was significantly greater than that of the other specimens. This is believed to be a result of the initiation of cracks in specimen ED3 at a closer distance to the column end, which resulted in a decreased rotation of the column with respect to the beam, leading to a larger flexural deformation of the column in the flexural hinge location. Moreover, based on the equivalent stiffness results at the point of a 20% drop in the strength, it can be observed that the three specimens exhibited similar stiffness.

4.5. Residual drift

Residual drift is a key factor in assessing the functionality of a structure after cyclic loading, as it can indicate whether the structure can still be safely used. The residual drift is a measure of the deformation or displacement that remains in a material or structure after it has been subjected to a cyclic load. To obtain the residual drift of a structure, the hysteretic loops can be analysed at each level when there is no lateral load present. Fig. 14 shows the residual drift at each drift ratio for the first cycle of the loading. The results indicate that the three specimens have low residual drift up to a drift ratio equal to 4%. However, specimen ED2 exhibited the lower residual drift of 0.23% while specimen ED1 exhibited the highest residual drift of 0.51%. These low values of residual drift are attributed to the linear elastic behaviour of GFRP bars which indicate the functionality of the structure after cyclic loading and minimize the required repair. After the drift ratio exceeds 4%, a significant variation in the residual drift is noticed. Specimen ED3 has the largest value of the residual drift followed by specimen ED1 while specimen ED2 has the lowest drift ratio for the corresponding drift ratio. Moreover, at the point of a 20% drop in the strength, it has been observed that ED3 exhibited the highest residual drift of 2.49%, followed closely by ED2 with a residual drift of 2.35%. The specimen ED1 displayed the lowest residual drift of 2.14%. It is evident that at the point of a 20% drop in the strength, the three specimens display a closer value of the residual drift. However, specimen ED3 may be slightly more susceptible to deformation or displacement under repeated loading compared to ED2 and ED1.

4.6. Beam rotation

Fig. 15 shows the beam rotation for the test specimens. The rotation of the beam was determined by dividing the vertical displacement at the cantilever end of the beam (measured using the vertical LVDT (3) in Fig. 6 by the distance between the LVDT#3 (see Fig. 6) and the first clamping point (approximately 670 mm), beyond which no rotation was assumed to occur. Fig. 15 reveals that the beam rotation was about 1.15% in specimens ED1 and 0.80% for the specimens ED2, but it

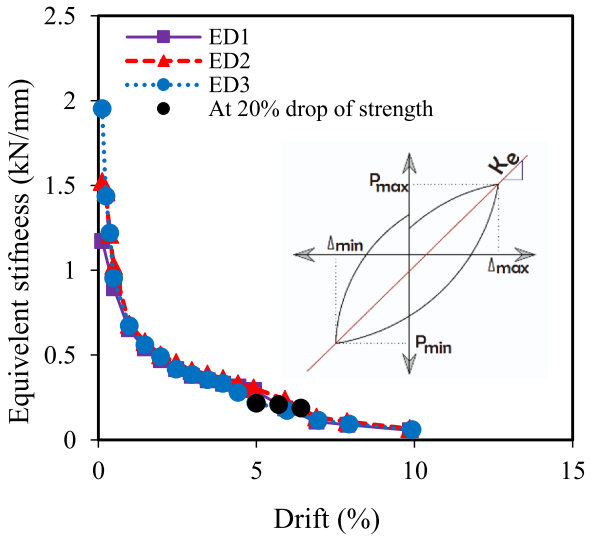

Fig. 13. Equivalent stiffness for the tested specimens.

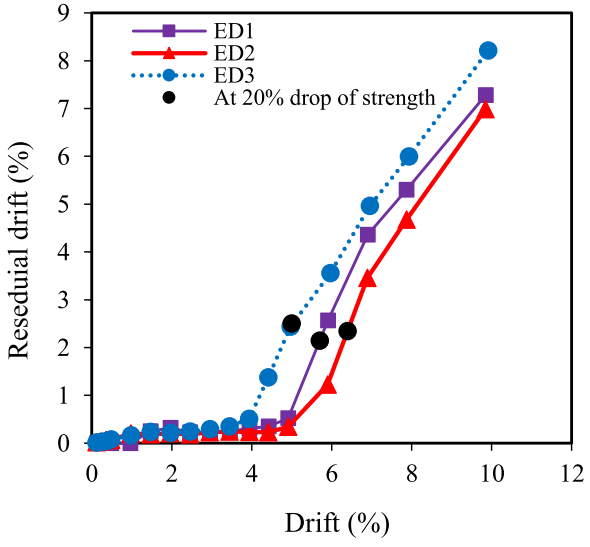

Fig. 14. Residual drift for the tested specimens.

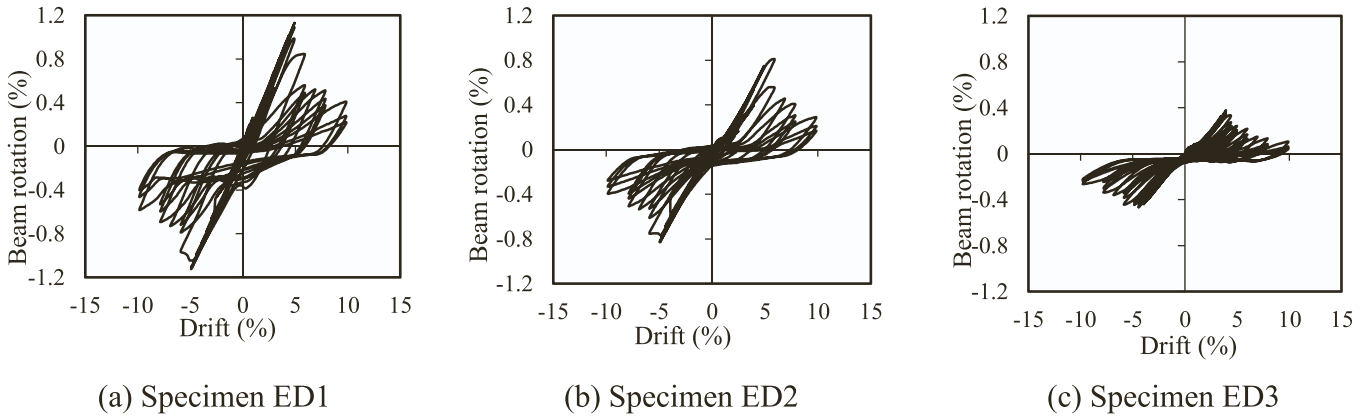

Fig. 15. Rotation of the beam.

significantly decreased to 0.40% in specimens ED3, indicating a less stiff connection. The higher beam rotation for specimen ED1 was attributed to an enhanced moment transferring mechanism between the column and beam, as a result of an improved connection integrity. This observation is in good agreement with the literature where smaller diameters of bonded GFRP bars with epoxy have better integrity and improved bond condition [44]. Additionally, Fig. 15 indicates that the beam rotation decreased after peak rotation, caused by connection softening, reducing the moment transferring capacity of the connections. Notably, specimen ED3 exhibited the least beam rotation at earlier drifts compared to other specimens. Due to the formation of plastic hinges at earlier stages and a poor contribution of prestressed GFRP bolts with nuts for transferring loads at larger drifts. This reduced beam rotation accounts for the reduced capacity of specimen ED3 compared to the other specimens.

4.7. Strain of connection reinforcement

Fig. 16 shows the strains developed in the connection reinforcement, measured using strain gauges attached longitudinally to the reinforcement. All specimens showed a similar trend for strain profile. The stain in all specimens is less than the rapture stain of GFRP bars indicating no failure of the reinforcement was observed. Moreover, the strain in specimen ED1 was the largest among the three specimens. This observation is compatible with the results presented earlier showing a better performance of GFRP bars in Specimens ED1. The maximum strain in the non-prestressed bolts of specimen ED2 was found to be 66% of that in specimen ED1. Although the bolt was prestressed in ED3, the total strain in the bolt was limited due to cracks, deformations, and plastic hinge formation closer to the connection, hindering further load transmission and limiting prestressing effectiveness. Comparing the results of specimens ED2 and ED3, which have identical amounts of reinforcement and identical bolts, the maximum strain was equal to 60% compared to specimen ED2. This agrees with the reduced capacity of specimen ED3 compared to ED2. Additionally, the strain magnitude at drift ratio up to 3% was approximately the same, after this value, the stain of specimen ED2 significantly increased while specimen ED3 was unable to exhibit greater values. However, both specimens ED1 and ED2 suffered a significant drop in the bar's stain after reaching the maximum strain value due to the softening behaviour of the connection.

5. Performance of epoxy duct connection in comparison to the pocket connection

As mentioned earlier, this study compares the behaviour of cap beam-to-column connections in precast GFRP-RC jetties. The pocketless connections proposed in this study had the same geometry as the pocket connections reported previously [35]. The performance of epoxy duct connections ED1 and ED2 in this study is compared to identical connections with pocket connections presented in a previous study [35]. The size and material properties of the specimens were similar to the ones presented; however, pocket connections were used to connect the beam and column elements. The performance of the pocket connection was found to depend on the depth of the column embedded into the pocket region (pocket depth). In the following, the behaviour of two specimens with pocket connections, EE3 and EE5, which were reported in [35], is compared to the results of the pocketless connections tested in the current study. The compression is presented in terms of backbone curves, energy dissipation, damping ratio, stiffness, and residual drifts.

5.1. Envelope curves

A comparison between the envelope curves for the current epoxy duct connections and identical pocket connections tested by [35] is

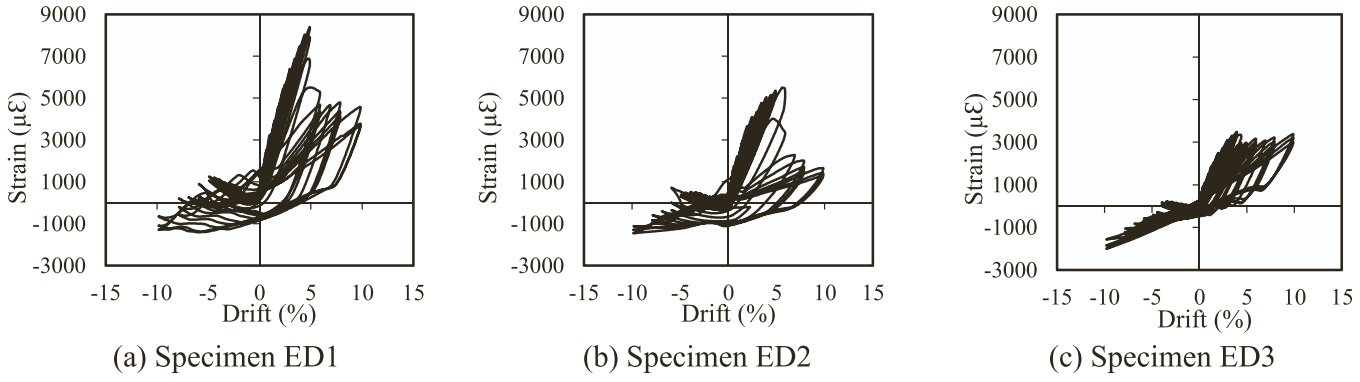

Fig. 16. Strains of the connectors.

shown in Fig. 17. The column reinforcement, dimensions, and material properties for both pocket connections EE3 and EE5 were the same as that of epoxy duct connections ED1 and ED2. Specimen EE5 had one bolt at the pocket region and overhanging distance of 200 mm while connection EE3 had an overhanging distance of 100 mm. The embedded depth of both specimens was equal to the column thickness. The results shown in Fig. 17 demonstrate the significant advantages of epoxy duct connections compared to pocket connections. The capacity of the pocketless connections ED2 was higher than that of the pocket connections EE5 and EE3 by 41% and 48%, respectively where the capacity of the pocket connections EE5 and EE3 was 15.22 kN and 14.45 kN, respectively. This reduced capacity of pocket connections is attributed to the governing failure mode of these connections. It was reported that pocket connections failed at the pocket location which caused the columns not to reach their maximum capacity, as shown in Fig. 18 [35]. In addition, the maximum capacity of the pocket connections was obtained at early drift ratios indicating a poor deformation capacity of this type of connection. An improvement for the pocket connection should be made to enhance the performance of these connections such as increasing the column embedded depth within the pocket.

5.2. Energy dissipation and damping ratio

Fig. 19-a shows the relationship between the drift ratio and the cumulative energy dissipation. The results show that both pocket and epoxy duct connections followed a similar trend where the energy dissipation increased with the increase of the drift ratio. The results demonstrated that epoxy duct connections had higher cumulative energy dissipation. The dissipated energy at the point of failure (strength drops by 20%) for pocket connections EE5 and EE3 was only 45% and 33% of that in the epoxy duct connection ED2. Moreover, the equivalent damping ratio shown in Fig. 19-b indicates that the pocket connections have a greater equivalent damping ratio at early loading due to the development of more cracks at the beginning of the loading compared to epoxy duct connections. However, at the point of a 20% drop in strength, the damping ratio of epoxy duct connections was found to be greater than that of pocket connections. The excessive damping after this point for pocket connections is due to premature failure at the pocket. In epoxy duct connections, a higher damping ratio was necessary to effectively dissipate energy. However, this leaves less leeway for allowing excessive damping. Consequently, the final damping ratio in epoxy duct connections was lower compared to the excessive damping ratio commonly seen in pocket connections.

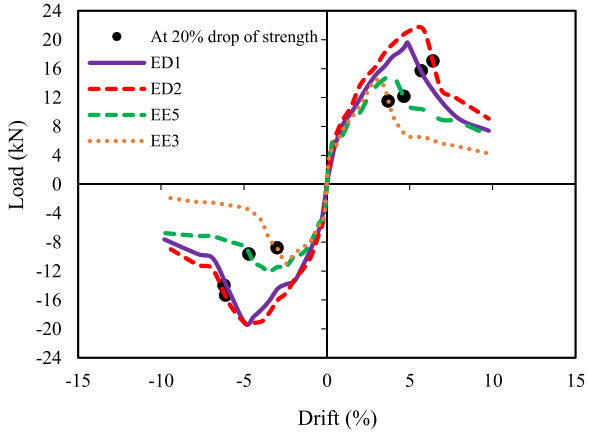

Fig. 17. Envelope curves for epoxy duct connections in comparison to pocket connections.

5.3. Stiffness deterioration

The equivalent stiffness obtained from the test specimens provides valuable insights into the behaviour of epoxy duct connections and pocket connections under cyclic loading, Fig. 20. At the beginning of loading, the pocket connections showed a greater equivalent stiffness compared to epoxy duct connections. However, after a drift ratio of 4%, the epoxy duct connections showed greater equivalent stiffness. This demonstrates the high rate of loss of stiffness for pocket connections which means that the pocket connections were unable to resist deformations over repeated cyclic loading. This high rate of stiffness loss is attributed to the stress concentration at the pocket that causes premature failure. Moreover, the damage accumulation in pocket connections can be concentrated in a few critical regions, leading to a faster reduction in stiffness. On the other hand, the provision of GFRP connectors in the ducts of epoxy duct connection led to more distributed damage and crack formation, resulting in a slower reduction in stiffness. Hence, the results indicate that epoxy duct connections may have a slight advantage in terms of equivalent stiffness under cyclic load.

5.4. Residual drift

A comparison between the residual drift for the epoxy duct connections and the pocket connections is shown in Fig. 21. The results show that up to a drift ratio of 3%, the residual drift for both types of connection is similar. At this range of drift ratios, the value of residual drift was very small due to the linear elastic behaviour of GFRP. After this point, the pocket connection exhibited a higher residual drift ratio at earlier cycles of loading. In general, the residual drift for pocket connections was found to be greater than that of epoxy duct connections. The difference in the observed residual drift depends on the mechanisms of energy dissipation and damage accumulation. The stress concentration, developed cracks, damage accumulation, and depending on the pocket location, in addition to the high rate of stiffness loss resulted in a larger residual drift at earlier drift ratios. Moreover, the epoxy duct connections can provide a more uniform stress distribution along the length of the bars, which can help in mitigating stress concentration and the formation of localized damage. The uniform stress distribution led to a more uniform and gradual reduction in stiffness during the loading cycles, resulting in a lower residual drift.

6. Conclusions

This study presents an experimental investigation of the cyclic behaviour of precast GFRP-RC connections using epoxy resin and connecting reinforcement in ducts. Three connections with different connector types including GFRP bars and pre-stressed and non-prestressed bolts were examined. The epoxy resin was utilized to bond the GFRP connectors within the prefabricated ducts in the beam and column. A unique test setup was employed to test the specimens under reversed cyclic loading that enabled the detection of the beam rotation. The cyclic performance of the proposed connections was also compared to identical precast pocket connections. The following outcomes can be drawn from this study:

1. The epoxy duct connections in the form of connection reinforcement in ducts is an efficient method that can used to accelerate the construction.
2. Pocketless GFRP-RC connections using epoxy resin and connecting reinforcement in ducts can reach a drift ratio of 4% without failure and strength reduction. This is due to the proper integrity of the structure that caused the shifting of the failure zone away from the connection interface.
3. The epoxy duct connection using GFRP bars or non-prestressed GFRP bolts had improved strength, energy dissipation, damping ratio

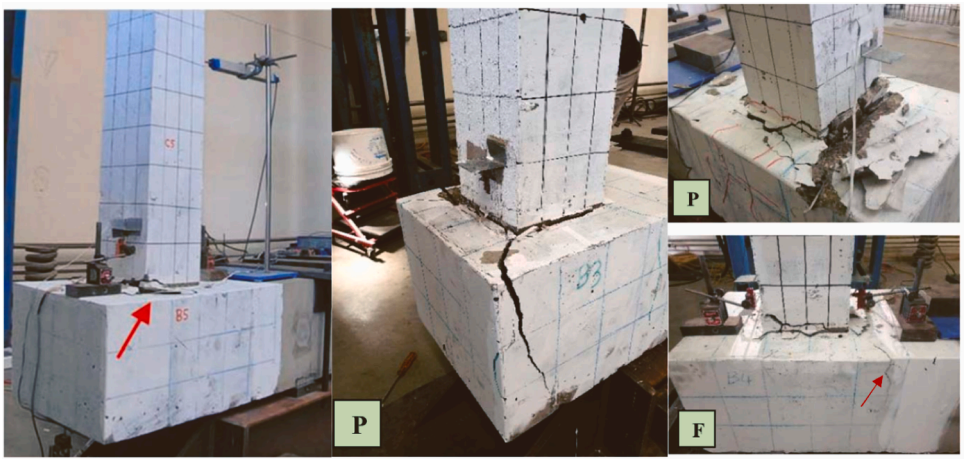

Fig. 18. Failure mode of pocket connections [35].

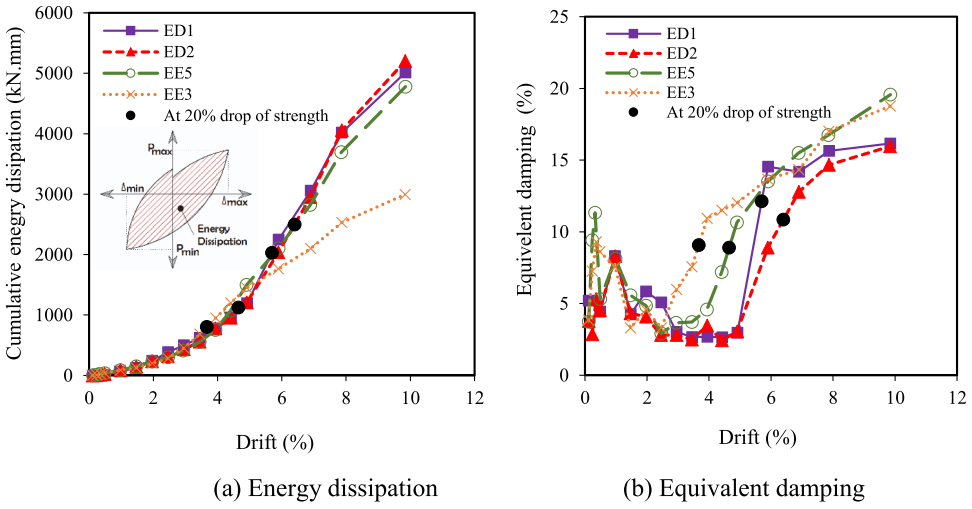

Fig. 19. Energy dissipation and equivalent damping for epoxy duct connections in comparison to pocket connections.

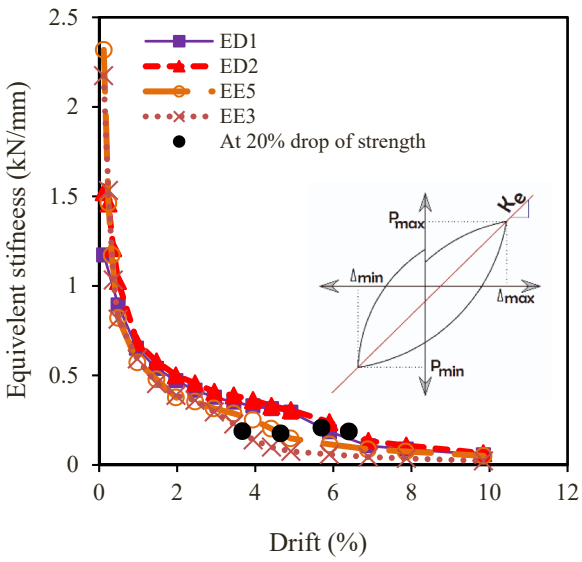

Fig. 20. Equivalent stiffness for epoxy duct connections in comparison to pocket connections.

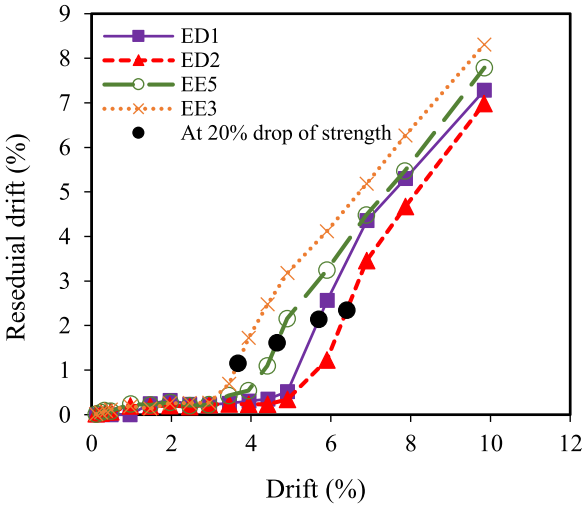

Fig. 21. Residual drift for epoxy duct connections in comparison to pocket connections.

stiffness, and residual drift compared to the connection with pre-stressed GFRP bolts with a nut.
4. Pocketless connection with GFRP bars had greater beam rotation and maximum strain of the connection reinforcement than using GFRP bolts and prestressed bolts. This is due to the smaller size of the used GFRP bars that can achieve better structure integrity compared to larger size bolts.
5. Epoxy duct connections can potentially prevent the premature failure observed in pocket connections—attributed to stress concentration and damage accumulation around the pocket. As opposed to the pocket connections, failure of the columns was observed in the pocketless epoxy duct connections presented in this study rather than the premature failure of the connection region. This indicates a stronger connection, as epoxy duct connections provide a more uniform transfer mechanism along the bars, thereby reducing stress concentration and localized damage formation.
6. Epoxy duct connections outperformed the pocket connections with improved behaviour in terms of drift capacity, energy dissipation, equivalent stiffness, and residual drift. The epoxy duct connections demonstrated a 48% higher capacity compared to pocket connections, along with a lower rate of stiffness deterioration.

While the results of this study can be applied to enhance the integrity of precast structures, gaining the benefits of accelerated durable construction, the application of these findings is limited to the specific type of epoxy used and the lengths of the connection reinforcement. To ensure the widespread application of this promising connection type, further studies are recommended. It is recommended to investigate the effect of different types of epoxies, various lengths, and bar diameters to develop an analytical model capable of determining the connection capacity and providing the optimum connection details. Additionally, adjustments to the test setup are suggested to enable the application of axial loads, thereby extending the application of this connection method to various structures, such as bridges.

Declaration of Competing Interest

The authors declare that they have no known competing financial interests or personal relationships that could have appeared to influence the work reported in this paper.

References

[1] Crespi P, Zucca M, Valente M, Longarini N. Influence of corrosion effects on the seismic capacity of existing RC bridges. Eng Fail Anal 2022;140:106546.
[2] Croce P., Formichi P., Landi F. Influence of reinforcing steel corrosion on life cycle reliability assessment of existing RC buildings. Buildings. 2020;10:99.
[3] GangaRao HV, Taly N, Vijay P. Reinforced concrete design with FRP composites. CRC Press; 2006.
[4] Pavlović A, Donchev T, Petkova D, Staletović N. Sustainability of alternative reinforcement for concrete structures: Life cycle assessment of basalt FRP bars. Constr Build Mater 2022;334:127424.
[5] Lai M, Liang Y, Wang Q, Ren F, Chen M, Ho J. A stress-path dependent stress-strain model for FRP-confined concrete. Eng Struct 2020;203:109824.
[6] Abbood IS. Properties evaluation of fiber reinforced polymers and their constituent materials used in structures–a review. Mater Today: Proc 2021;43:1003–8.
[7] Gouda MG, Mohamed HM, Manalo AC, Benmokrane B. Effect of transverse reinforcement ratios and configurations on the behavior of hollow circular concrete columns reinforced with GFRP under concentric loading. J Compos Constr 2023;27:04022095.
[8] Hassanli R, Manalo A, Vafaei D, Yekrangnia M, Elchalakani M, Noël M. Cyclic behavior of GFRP-reinforced concrete one-way slabs with synthetic fibers. J Build Eng 2023;65:105741.
[9] Krall M, Polak M. Concrete beams with different arrangements of GFRP flexural and shear reinforcement. Eng Struct 2019;198:109333.
[10] Murthy AR, Pukazhendhi D, Vishnuvardhan S, Saravanan M, Gandhi P. Performance of concrete beams reinforced with GFRP bars under monotonic loading. Structures 2020:1274–88.
[11] Paulay T. Joints in Reinforced Concrete Frames Designed Earthquake Resistance. U SN Z-Japan Seminar Report1984.
[12] Kurama YC, Sritharan S, Fleischman RB, Restrepo JI, Henry RS, Cleland NM, et al. Seismic-resistant precast concrete structures: State of the art. J Struct Eng 2018;144:03118001.
[13] El-Naqeeb MH, Abdelwahed BS. Nonlinear finite element investigations on different configurations of exterior beam-column connections with different concrete strengths in column and floor. Structures 2023;50:1809–26.
[14] Ghomi SK, El-Salakawy E. Effect of joint shear stress on seismic behaviour of interior GFRP-RC beam-column joints. Eng Struct 2019;191:583–97.
[15] Mady M, El-Ragaby A, El-Salakawy E. Seismic behavior of beam-column joints reinforced with GFRP bars and stirrups. J Compos Constr 2011;15:875–86.
[16] Ghomi SK, El-Salakawy E. Seismic behavior of GFRP-reinforced concrete interior beam–column–slab subassemblies. J Compos Constr 2019;23:04019047.
[17] Ghomi SK, El-Salakawy E. Seismic behavior of exterior GFRP-RC beam–column connections: analytical study. J Compos Constr 2018;22:04018022.
[18] Lin G, Zeng J-J, Liang S-D, Liao J, Zhuge Y. Seismic behavior of novel GFRP bar reinforced concrete beam-column joints internally reinforced with an FRP tube. Eng Struct 2022;273:115100.
[19] Safdar M, Sheikh MN, Hadi MN. Cyclic performance of GFRP-RC T-connections with different anchorage and connection details. J Compos Constr 2022;26:04022022.
[20] Elliott KS. Precast concrete structures. Crc Press; 2019.
[21] Nanyam VN, Basu R, Sawhney A, Vikram H, Lodha G. Implementation of precast technology in India–opportunities and challenges. Procedia Eng 2017;196:144–51.
[22] Camarena C., Saiidi M.S., Moustafa M. Column and Footing Pocket Connections for Cast-in-Place and Precast Construction. 2021.
[23] M.S. Saiidi M. Mehraein G. Shrestha E. Jordan A. Itani M. Tazarv et al. Proposed AASHTO seismic specifications for ABC column connections2020.
[24] Zhang Y, Li D. Seismic behavior and design of repairable precast RC beam–concrete-filled square steel tube column joints with energy-dissipating bolts. J Build Eng 2021;44:103419.
[25] Tullini N, Minghini F. Cyclic test on a precast reinforced concrete column-to-foundation grouted duct connection. Bull Earthq Eng 2020;18:1657–91.
[26] Ghayeb HH, Razak HA, Sulong NR. Seismic performance of innovative hybrid precast reinforced concrete beam-to-column connections. Eng Struct 2020;202:109886.
[27] Zhang R, Zhang Y, Li A, Yang T. Experimental study on a new type of precast beam-column joint. J Build Eng 2022;51:104252.
[28] Wang Z, Wang J, Liu J, Han F, Zhang J. Large-scale quasi-static testing of precast bridge column with pocket connections using noncontact lap-spliced bars and UHPC grout. Bull Earthq Eng 2019;17:5021–44.
[29] Tazarv M, Saiidi MS. Design and construction of UHPC-filled duct connections for precast bridge columns in high seismic zones. Struct Infrastruct Eng 2017;13:743–53.
[30] Zhou Y, Ou Y-C, Lee GC. Bond-slip responses of stainless reinforcing bars in grouted ducts. Eng Struct 2017;141:651–65.
[31] Fan J-J, Feng D-C, Wu G, Hou S, Lu Y. Experimental study of prefabricated RC column-foundation assemblies with two different connection methods and using large-diameter reinforcing bars. Eng Struct 2020;205:110075.
[32] Wang Z, Wu C, Li T, Xiao W, Wei H, Qu H. Experimental study on the seismic performance of improved grouted corrugated duct connection (GCDC) design for precast concrete bridge column. J Earthq Eng 2022;26:2469–90.
[33] ACI CODE-. 440.11–22: Building Code Requirements for Structural Concrete Reinforced with Glass Fiber-Reinforced Polymer (GFRP) Bars—Code and Commentary. American Concrete Institute; 2023.
[34] Ngo TT, Pham TM, Hao H, Chen W, San Ha N. Proposed new dry and hybrid concrete joints with GFRP bolts and GFRP reinforcement under cyclic loading: testing and analysis. J Build Eng 2022;49:104033.
[35] Ghanbari-Ghazijahani T, Hassanli R, Manalo A, Smith ST, Vincent T, Gravina R, et al. Cyclic behavior of beam–column pocket connections in GFRP-reinforced precast concrete assemblages. J Compos Constr 2023;27:04022107.
[36] El-Naqeeb MH, Hassanli R, Zhuge Y, Ma X, Manalo A. Numerical investigation on the behaviour of socket connections in GFRP-reinforced precast concrete. Eng Struct 2024;303:117489.
[37] Hassanli R, Vincent T, Manalo A, Smith ST, Gholampour A, Gravina R. Large-scale experimental study on pocket connections in GFRP-reinforced precast concrete frames. Structures 2021:523–41.
[38] Hassanli R, Vincent T, Manalo A, Smith ST, Gholampour A, Gravina R, et al. Connections in GFRP reinforced precast concrete frames. Compos Struct 2021;276:114540.
[39] Guide for the Design and Construction of Structural Concrete Reinforced with Fiber-Reinforced Polymer Bars. American Concrete Institute; 2015.
[40] ASTM. Standard test methods for cyclic (reversed) load test for shear resistance of vertical elements of the lateral force resisting systems for buildings. ASTM E2126. 2011.
[41] Sagar B. MVN S. Mechanical and microstructure characterization of alccofine based high strength concrete. Silicon 2021:1–19.
[42] S806:12C. Design and construction of building structures with fibre-reinforced polymers. Ontario, Canada: Canadian Standards Association; 2012.
[43] Jacobsen LS. Steady forced vibration as influenced by damping. Trans ASME 1930;52.
[44] Caro M, Jemaa Y, Dirar S, Quinn A. Bond performance of deep embedment FRP bars epoxy-bonded into concrete. Eng Struct 2017;147:448–57.